Scientific Research Publishing

Advances in Chemical Engineering and Science, 2022, 12, 54-64
https://www.scirp.org/journal/aces
ISSN Online: 2160-0406
ISSN Print: 2160-0392

Influence of Photon Pump Fluence on Charge Carriers in $FAPbI_3$ and Manganite Perovskites

Nam Joong Jeon[1], Jangwon Seo[1*], Sanghee Nah[2], Jung-Keun Lee[3*]

[1]Division of Advanced Materials, Korea Research Institute of Chemical Technology, Daejeon, Korea
[2]Seoul Center, Korea Basic Science Institute, Seoul, Korea
[3]Physics Department, Division of Liberal Arts and Sciences, Hanil University & PTS, Wanju, Korea
Email: *jwseo@krict.re.kr, *jklee@jbnu.ac.kr

How to cite this paper: Jeon, N.J., Seo, J., Nah, S. and Lee, J.-K. (2022) Influence of Photon Pump Fluence on Charge Carriers in $FAPbI_3$ and Manganite Perovskites. *Advances in Chemical Engineering and Science*, **12**, 54-64.
https://doi.org/10.4236/aces.2022.121005

Received: December 22, 2021
Accepted: January 18, 2022
Published: January 21, 2022

Copyright © 2022 by author(s) and Scientific Research Publishing Inc.
This work is licensed under the Creative Commons Attribution International License (CC BY 4.0).
http://creativecommons.org/licenses/by/4.0/

Open Access

Abstract

$FAPbI_3$ and $FA(Mn:Pb)I_3$ perovskite films were prepared and evaluated through steady and transient absorption spectroscopy. According to the analysis using Elliot's model, there were no considerable differences except for the absorption intensity between $FAPbI_3$ and $FA(Mn:Pb)I_3$ perovskite films: the value of the optical gap (E_g) and the position of exciton resonance (E_0) were the same. The femtosecond transient absorption showed biexponential relaxation properties of the charge carriers, suggesting that biexcitons are more easily generated in $FA(Mn:Pb)I_3$ than $FAPbI_3$ perovskite. The generation of biexcitons in $FA(Mn:Pb)I_3$ was also confirmed by the photon pump fluence dependence. Moreover, we were able to estimate the average number of absorbed photons $\langle N \rangle$ directly from the photon pump power dependence without needing any further experimental measurements such as photoluminescence. Our findings may offer a new way of understanding photoinduced carrier dynamics in perovskite manganites.

Keywords

$FAPbI_3$, Perovskite Manganites, Transient Absorption

1. Introduction

Formamidinium lead iodide ($FAPbI_3$) has attracted substantial attention [1]-[12]. The band gap of $FAPbI_3$ allows for broader absorption of the solar spectrum relative to $MAPbI_3$. A composite of $FAPbI_3$ and $MAPbBr_3$ layer obtained a power conversion efficiency exceeding 20% [6]. To date, perovskite solar cells (PSCs) with photo conversion efficiencies (PCEs) of >25% mainly use $FAPbI_3$-dominated

perovskite as a light absorber due to their superior opto-electrical properties, narrower band gap, longer charge-diffusion length, and better photostability and thermostability [12]. Meanwhile, perovskite manganites may provide a useful material platform for new magnetic materials [13]. MA(Mn:Pb)I_3 has been studied by Nafradi *et al.*, and they found that photo-excited electrons melt the local magnetic order in the ferromagnetic photovoltaic MA(Mn:Pb)I_3 [14]. Technologically relevant materials may emerge when magnetic interactions of spins are present and competing to determine the ground state [15]. This may provide potential for realizing magnetic bits, information storage, and increased manipulation speed [14] [16] [17]. A deeper understanding of charge generation, exciton dissociation, trapping and recombination in photovoltaic manganite perovskites is needed to unravel the operating mechanism.

In this work, we report on studies examining $FAPbI_3$ and manganite FA(Mn:Pb)I_3 perovskite films using static and transient absorption spectroscopy to explore charge carrier generation, relaxation, and photon fluence dependence. We used femtosecond transient absorption (TA) spectroscopy to investigate the dynamics of the carriers [18]. The measurements were carried out under various pump fluences, and Poisson statistics were used to interpret the data. We found no considerable differences in the optical gap (E_g) or the position of exciton resonance (E_0) between FA(Mn:Pb)I_3 and $FAPbI_3$. Biexcitons were considered to be more easily generated in FA(Mn:Pb)I_3 than $FAPbI_3$. There was a difference in photon pump power dependence between the biexcitons and single excitons generated in FA(Mn:Pb)I_3 and $FAPbI_3$, respectively. Meanwhile, we were able to estimate the value of the average number of absorbed photons $<N>$ directly from the pump power-dependence without needing further optical measurements such as photoluminescence (PL) [18] [19] [20].

2. Samples and Measurements

The fabrication of the $FAPbI_3$ and FA(Mn:Pb)I_3 thin films with thickness of about 400 nm has been carried out through two-step sequential deposition and solvent engineering representative of wet processes that can yield perovskite films for high-performance perovskite solar cells. $FAPbI_3$ films were synthesized as described in previous publications [6] [10]. For the mixed halide perovskite FA(Mn:Pb)I_3 films, details are referred from a reference [14]. Femtosecond transient absorption measurements were carried out with the Femtosecond Multidimensional Laser Spectroscopic System (FMLS) at the Korea Basic Science Institute.

3. Results and Discussion

The absorption spectrum in direct semiconductors near the bandgap can be described using the Elliott formula [21]-[26], where the contributions of discrete exciton transitions are added to the continuum transitions [22] [23] [25] [26]. **Figure 1(a)** shows the absorption spectrum of a $FAPbI_3$ film near the optical gap

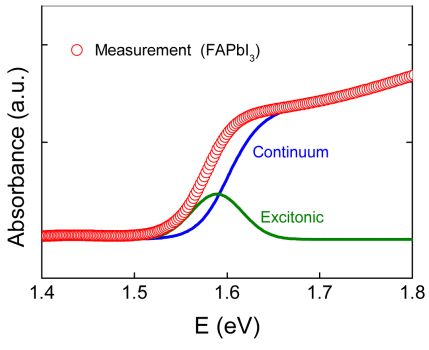

(a)

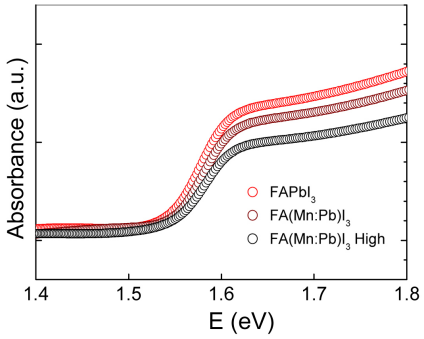

(b)

Figure 1. (a): Absorption spectrum and Elliott's model of the $FAPbI_3$ films. The absorption spectrum (red circles) near the bandgap was fit by Elliott's model. The contribution from excitonic (green dashed line) and continuum band (blue dash line) transitions are also plotted. (b): Absorption spectra of the $FA(Mn:Pb)I_3$ films compared with $FAPbI_3$. "$FA(Mn:Pb)I_3$ High" refers to $FA(Mn:Pb)I_3$ with high Mn concentration.

at room temperature. We have analyzed the absorption spectra in this study using Elliot's formula:

$$A(\omega) = A_0 \cdot \theta(\hbar\omega - E_g) \cdot \left(\frac{\pi e^{\pi x}}{\sinh(\pi x)} \right) + A_0 \cdot R_{ex} \sum_{n_{ex}=1}^{\infty} \frac{4\pi}{n_{ex}^3} \cdot \delta\left(\hbar\omega - E_g + R_{ex}/n_{ex}^2\right) \quad (1)$$

where A_0 is a constant related to the transition matrix element; ω is the frequency of light, θ is the step function; E_g is the bandgap; x is defined as $R_{ex}^{1/2} / \left(\hbar\omega - E_g\right)^{1/2}$, where R_{ex} is the exciton binding energy; n_{ex} is the principal quantum number; and δ denotes a delta function. To account for inhomogeneous broadening, the continuum and excitonic part of Equation (1) are convolved with Gaussian functions with standard deviations. The standard deviation of the exitonic part Gaussian function was found to be 23.9 meV. A model based on Elliott's formula reproduced the spectra very well. In **Figure 1(a)**, an excitonic absorption peak appears just below the bandgap energy, while on the high-energy side of the exciton peak, the absorbance shows a plateau with a slight slope, which is attributed to the continuum contribution described by the first term of the right-hand side of Equation (1). From the best fitting of the model, we ex-

tracted that the exciton resonance (E_0) is centered at 1.589 eV. The exciton resonance of 1.589 eV is smaller than that (1.631 eV) in $MaPbI_3$ [26]). The bandgap (E_g) of continuum transitions was found at 1.60 eV, which is consistent with recently reported values (1.48 - 2.43 eV) for $FAPbI_3$ [3] [12]. The bandgap (E_g) at 1.60 eV yields an exciton binding energy ($R_{ex} = E_g - E_0$) of 11 meV (which is the same as that (11 meV) in $MAPbI_3$ [26]. **Figure 1(b)** shows the absorbance spectra of $FA(Mn:Pb)I_3$ films compared with the measurement of $FAPbI_3$. The spectra of the $MA(Mn:Pb)I_3$ films show no distinguishable difference between them except the reduced intensities with increased Mn concentrations. Elucidating the role of excitons and free carriers in these materials would provide a deeper understanding of the mechanisms that give rise to the exceptional performance of hybrid perovskite-based devices [27]. Although the absorption coefficient was smaller, the other parameters were the same. We used the same exciton binding energy (R_{ex} = 11 meV) and bandgap (E_g = 1.60 eV) used for the $FAPbI_3$ to fit the data [9]. Increased Mn content may have caused changes in absorption intensity [28]-[34].

Figure 2 shows the relaxation of transient absorption ($\Delta T/T$), which was measured at the power of 0.16 μW for $FAPbI_3$ and $FA(Mn:Pb)I_3$ films, normalized at the initial maximum points. The decay essentially reflects the temporal evolution of the charge carrier density while assuming that the carrier mobilities are unchanged [35]. The different relaxation pattern suggests that there are both fast (with τ_1) and slow (with τ_2) components. Thus, the relaxation of the transmission signals can be fitted to a biexponential decay. Therefore, we used the equation, $y(t) = A_1 e^{-\frac{t}{\tau_1}} + A_2 e^{-\frac{t}{\tau_2}} + C$ to analyze the relaxation data [18] [36]. For the $FA(Mn:Pb)I_3$ sample, we obtained $y_{FA(Mn:Pb)I_3}(t) = 0.108e^{-\frac{t}{362\,ps}} + 0.281e^{-\frac{t}{843\,ps}} + 0.62$ for the best fit. For the $FAPbI_3$ sample, we obtained $y_{FAPbI_3}(t) = 0.054e^{-\frac{t}{132\,ps}} + 0.254e^{-\frac{t}{961\,ps}} + 0.7$.

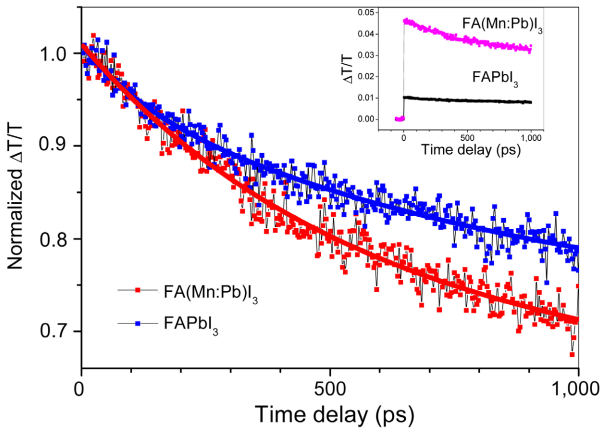

Figure 2. Normalized Transient transmission changes of $FAPbI_3$ and $FA(Mn:Pb)I_3$, pumped at 400 nm and probed at 720 nm on picosecond time scales. Inset: $\Delta T/T$ relaxation, unnormalized.

In semiconductor nanoparticles, one can generate states in which several excitons occupy a volume comparable to or smaller than that of a bulk exciton [16]. The fast relaxation is known to be originated from the biexcitons, while the slow relaxation is attributed to single excitons [18] [19] [20] [37]. The experimental detection of strongly confined multiexcitons is usually associated with their very short (picoseconds to hundreds of picoseconds) lifetimes, which are limited by nonradiative Auger recombination [16]. We aimed to determine the possible existence of trions by assigning triple exponential decays [18], but we did not find any success. So, we simplified it to biexponential decay, as opposed to triple exponential decay which includes trions. Therefore, we regarded simply that the intensity of the fast component (A_1) can be mainly attributed to the biexcitons. Our result suggests that biexcitons are more easily generated in $FA(Mn:Pb)I_3$ than in $FAPbI_3$ (since $A_{1M} = 0.108 > A_{1F} = 0.054$) [16] [18].

To further clarify the origins of the major charge carriers immediately after photoexcitation, we investigated the photon pump fluence dependence of $\Delta T/T$ before the relaxation of the photoinduced charges was initiated. **Figure 3(a)** shows the photoinduced transient absorption ($\Delta T/T$) at different pump powers

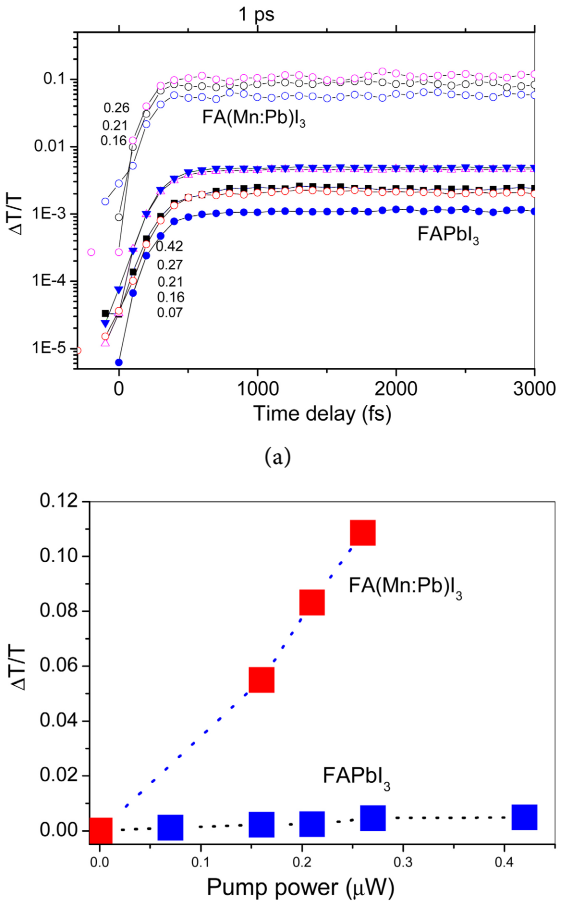

Figure 3. (a) TA of the $FAPbI_3$ and $FA(Mn:Pb)I_3$ perovskite films at differing pump powers as indicated by the numbers in the unit of μW. (b) $\Delta T/T$ vs. photon pump power.

[18] [36] for early short times (<3 ps) for (a) FA(Mn:Pb)I_3 and (b) $FAPbI_3$. The TA signals rise instantaneously after photoexcitation in about ~0.5 ps (which is the proper instrument response time), then reach their peak, at which they are saturated and stable. We only measured for the first 5 ps time scale before the appearance of fast relaxation. For long delays, only single excitons would be left. In **Figure 3(b)**, the values of $\Delta T/T$ are plotted as a function of the excitation laser power, and a fit is presented as a visual guide. It is expected that biexcitons are more easily generated with increasing power in FA(Mn:Pb)I_3, while excitons are mainly generated in $FAPbI_3$. This is comparable to the behavior of perovskite films with well-defined band edges [37].

To ascertain whether the generated charges in FA(Mn:Pb)I_3 and $FAPbI_3$ films (**Figure 3**) are mostly biexciton dominant or exciton dominant, we have used Poisson statistics to analyze the results. According to the Poisson distribution, the probability of exciton (biexciton) generation [18] [19], $P_.$ ($P_{..}$) in nanocrystals, is described as follows:

$$P_.\left(j_{ex}\right)=1-\mathrm{e}^{-\sigma j_{ex}} \tag{2}$$

$$P_{..}\left(j_{ex}\right)=1-\mathrm{e}^{-\sigma j_{ex}}-\sigma j_{ex}\mathrm{e}^{-\sigma j_{ex}} \tag{3}$$

where j_{ex} is the excitation photon fluence and σ is the absorption cross-section of the material. The excitation photon fluence j_{ex} is determined by the pump power. We presumed that j_{ex} is proportional to photon pump power. The value of $\Delta T/T$ is related to the photon bleaching (PB) intensity. The PB intensity of excitons (biexcitons) is proportional to the number of excitons (biexcitons) generated in the material. Thus, we can plot $\Delta T/T$ related to the generation probability [18] [37] of the biexciton in FA(Mn:Pb)I_3 and the exciton in the $FAPbI_3$ sample, respectively. We therefore presumed that the amplitudes of TA can be expressed using the following equations.

$$\Delta T/T_{in\ FA}\left(X\right)\propto P_.\left(j_{ex}\right)=A_{FA}\left(1-\mathrm{e}^{-S\cdot X}\right) \tag{4}$$

$$\Delta T/T_{in\ MM}\left(X\right)\propto P_{..}\left(j_{ex}\right)=A_{MM}\left(1-\mathrm{e}^{-S\cdot X}-S\cdot X\mathrm{e}^{-S\cdot X}\right), \tag{5}$$

where X denotes the "*pump power*" and $X\equiv j_{ex}/k$, where k is an unknown factor. We set $S\equiv k\sigma$. Thus, $S\cdot X=\sigma j_{ex}=\langle N\rangle$, the average number of absorbed photons. The subscripts $_{\mathrm{FA}}$ and $_{\mathrm{MM}}$ respectively refer to $FAPbI_3$ and FA(Mn:Pb)I_3 film. A_{FA} and A_{MM} are unique proportional factors in the $FAPbI_3$ and FA(Mn:Pb)I_3 samples, respectively.

Thus, in **Figure 4(a)** and **Figure 4(b)**, the amplitudes of TA are plotted as a function of the pump power for different values of S. As shown in the log-log plot, only the slope matters in comparing the two different types of charges: biexciton or exciton. We obtained A_{MM} = 0.335 (**Figure 4(a)**) and A_{FA} = 0.003 (**Figure 4(b)**), and S = 4.5 was obtained to give the best fit for both. In **Figure 4(a)**, the generated charges in FA(Mn:Pb)I_3 exhibit an increase similar to that of the biexciton amplitude, while the charges in the $FAPbI_3$ sample show an increase following that of single exciton amplitude ($P_.$) in **Figure 4(b)**. This is

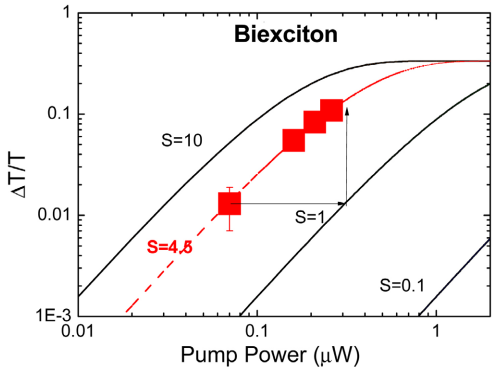

(a)

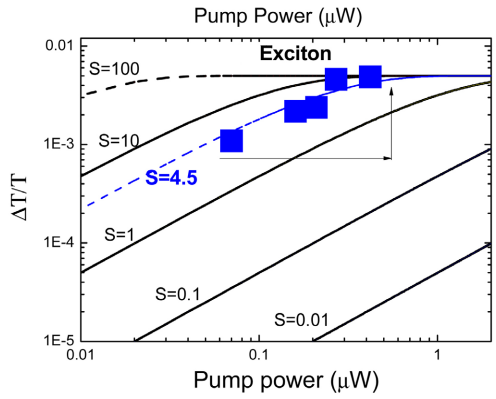

(b)

Figure 4. The power-dependence data (full squares) plotted on the predicted generation probability (solid lines) of photo-excited charge carriers for differing values of S ($S = \sigma j$) as a function of pump power (a) for biexciton, (b) for exciton.

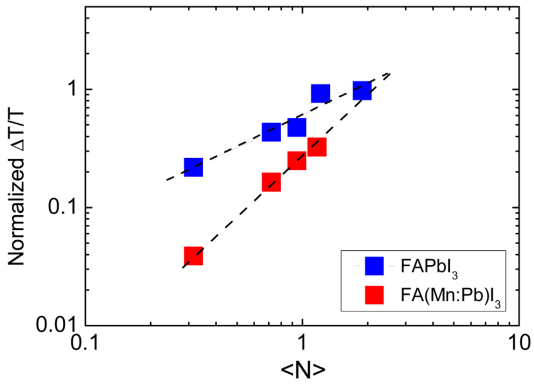

Figure 5. Normalized (to the maximum) $\Delta T/T$ as a function of $\langle N \rangle$.

consistent with the implication showing that the biexciton is more dominant in FA(Mn:Pb)I_3, which is not the case in $FAPbI_3$ (as shown in **Figure 2**) at low pump power.

Finally, in **Figure 5**, the normalized $\Delta T/T$ was depicted as a function of $\langle N \rangle$. To obtain the value of $\langle N \rangle$ here, we simply calculated $S \cdot X = \sigma j_{ex} = \langle N \rangle$ without the need for any further measurements such as the photon pump flu-

ence dependence of transient photoluminescence [18] [20] [37]. Our estimation of $\langle N \rangle$ is comparable to the previously reported experimental values of $\langle N \rangle$ which were obtained using similar transient absorption and PL methods [18] [19] [20].

4. Conclusion

In conclusion, $FAPbI_3$ and $FA(Mn:Pb)I_3$ perovskite films were prepared and evaluated through steady and transient absorption spectroscopy. There was no considerable variation in the absorption spectrum between the $FAPbI_3$ and $FA(Mn:Pb)I_3$ perovskite films, except for the absorption intensity in the steady absorption spectrum. The femtosecond transient absorption showed biexponential relaxation properties of the charge carriers, which suggested that biexcitons are more easily generated in $FA(Mn:Pb)I_3$ than $FAPbI_3$ perovskite; the generation of *biexcitons* was also confirmed by the photon pump fluence dependence. We estimated the average number of absorbed photons $\langle N \rangle$ directly from the photon pump power dependence without relying on any further experimental measurements such as PL. Our findings may offer a new way of understanding photoinduced carrier dynamics in perovskite manganites.

Acknowledgements

This research was supported by a grant from the Korea Research Institute of Chemical Technology (KRICT) (SS2122-20), and by the National Research Council of Science & Technology (NST) grant by the Korea government (MSIT) (No. CAP18054-200). This research was partly supported by the Basic Science Research Program through the National Research Foundation of Korea (NRF) funded by the Ministry of Education (2017R1D1A1B03028062). Femtosecond transient absorption measurements were carried out with the Femtosecond Multidimensional Laser Spectroscopic System (FMLS) at the Korea Basic Science Institute.

Conflicts of Interest

The authors declare no conflicts of interest regarding the publication of this paper.

References

[1] Kojima, A., Teshima, K., Shirai, Y. and Miyasaka, T. (2009) Organometal Halide Perovskites as Visible-Light Sensitizers for Photovoltaic Cells. *Journal of the American Chemical Society*, **131**, 6050-6051. https://doi.org/10.1021/ja809598r

[2] Lee, M.M., Teuscher, J., Miyasaka, T., Murakami, T.N. and Snaith, H.J. (2012) Efficient Hybrid Solar Cells Based on Meso-Superstructured Organometal Halide Perovskites. *Science*, **38**, 643-647. https://doi.org/10.1126/science.1228604

[3] Eperon, G.E., Stranks, S.D., Menelaou, C., Johnston, M.B., Herz, L.M. and Snaith, H.J. (2014) Formamidinium Lead Trihalide: A Broadly Tunable Perovskite for Efficient Planar Heterojunction Solar Cells. *Energy & Environmental Science*, **7**, 982-988. https://doi.org/10.1039/c3ee43822h

[4] Gao, N.P., Gregori, G., Yang, T.-Y., Nazeeruddin, M.K., Maier, J. and Gratzel, M. (2014) Mixed-Organic-Cation Perovskite Photovoltaics for Enhanced Solar-Light Harvesting. *Angewandte Chemie International Edition*, **53**, 3151-3157. https://doi.org/10.1002/anie.201309361

[5] You, J., Yang, Y., Hong, Z., Song, T.-B., Meng, L., Liu, Y., *et al.* (2014) Moisture Assisted Perovskite Film Growth for High Performance Solar Cells. *Applied Physics Letters*, **105**, Article ID: 183902. https://doi.org/10.1063/1.4901510

[6] Yang, W.S., Noh, J.H., Nam, J.J., Kim, Y.C., Ryu, S., Seo, J. and Seok, S.I. (2015) High-Performance Photovoltaic Perovskite Layers Fabricated through Intramolecular Exchange. *Science*, **348**, 1234-1237. https://doi.org/10.1126/science.aaa9272

[7] Piatkowski, P., Cohen, B., Kazim, S., Ahmad S. and Douhal, A. (2016) How Photon Pump Fluence Changes the Charge Carrier Relaxation Mechanism in an Organic-Inorganic Hybrid Lead Triiodide Perovskite. *Physical Chemistry Chemical Physics*, **18**, 27090-27101. https://doi.org/10.1039/C6CP02682F

[8] Targhi, F.F., Jalili, Y.S. and Kanjouri, F. (2018) $MAPbI_3$ and $FAPbI_3$ Perovskites as Solar Cells: Case Study on Structural, Electrical and Optical Properties. *Results in Physics*, **10**, 616-627. https://doi.org/10.1016/j.rinp.2018.07.007

[9] Gao, L., Spanopoulos, I., Ke, W., Huang, S., Hadar, I., Chen, L., Li, X., Yang, G. and Kanatzidis, M.G. (2019) Improved Environmental Stability and Solar Cell Efficiency of (MA,FA)PbI_3 Perovskite Using a Wide-Band-Gap 1D Thiazolium Lead Iodide Capping Layer Strategy. *ACS Energy Letters*, **4**, 1763-1769. https://doi.org/10.1021/acsenergylett.9b00930

[10] Jeon, N.J., Yang, T.-Y., Park, H.H., Seo, J., Nam, D.Y., Jeong, D., Hong, S., Kim, S.H., Cho, J.M., Jang, J.J. and Lee, J.-K. (2019) Thermally Activated, Light-Induced Electron-Spin-Resonance Spin Density Reflected by Photocurrents in a Perovskite Solar Cell. *Applied Physics Letters*, **114**, Article ID: 013903. https://doi.org/10.1063/1.5053830

[11] Qiao, L., Sun, X. and Long, R. (2019) Mixed Cs and FA Cations Slow Electron-Hole Recombination in $FAPbI_3$ Perovskites by Time-Domain *Ab Initio* Study: Lattice Contraction versus Octahedral Tilting. *The Journal of Physical Chemistry Letters*, **10**, 672-678. https://doi.org/10.1063/1.5053830

[12] Chen, Z., Zhang, H., Yao, F., Tao, C., Fang, G. and Li, G. (2020) Room Temperature Formation of Semiconductor Grade α-$FAPbI_3$ Films for Efficient Perovskite Solar Cells. *Cell Reports Physical Science*, **1**, Article ID: 100205. https://doi.org/10.1016/j.xcrp.2020.100205

[13] Xia, W., Pei, Z., Leng, K. and Zhu, X., (2020) Research Progress in Rare Earth-Doped Perovskite Manganite Oxide Nanostructures. *Nanoscale Research Letters*, **15**, Article No. 9. https://doi.org/10.1186/s11671-019-3243-0

[14] Náfrádi, B., Szirmai, P., Spina, M., Lee, H., Yazyev, O.V. and Arakcheeva, A. (2016) Optically Switched Magnetism in Photovoltaic Perovskite CH_3NH_3(Mn: Pb)I_3. *Nature Communications*, **7**, Article No. 13406. https://doi.org/10.1038/ncomms13406

[15] Cui, B., Song, C., Wang, G., Yan, Y., Peng, J., Miao, J., *et al.* (2014) Reversible Ferromagnetic Phase Transition in Electrode-Gated Manganites. *Advanced Functional Materials*, **24**, 7233-7240. https://doi.org/10.1002/adfm.201402007

[16] Achermann, M., Hollingsworth, J.A. and Klimov, V.I. (2003) Multiexcitons Confined within a Subexcitonic Volume: Spectroscopic and Dynamical Signatures of Neutral and Charged Biexcitons in Ultrasmall Semiconductor Nanocrystals. *Physical Review B*, **68**, Article ID: 245302. https://doi.org/10.1103/PhysRevB.68.245302

[17] Dey, A. and Yarlagadda, S. (2018) Temperature Dependence of Long Coherence

Times of Oxide Charge Qubits. *Scientific Reports*, **8**, Article No. 3487. https://doi.org/10.1038/s41598-018-21767-2

[18] Yarita, N., Tahara, H., Ihara, T., Kawawaki, T., Sato, R., Saruyama, M., Teranishi, T. and Kanemitsu, Y. (2017) Dynamics of Charged Excitons and Biexcitons in $CsPbBr_3$ Perovskite Nanocrystals Revealed by Femtosecond Transient-Absorption and Single-Dot Luminescence Spectroscopy. *The Journal of Physical Chemistry Letters*, **8**, 1413-1418. https://doi.org/10.1021/acs.jpclett.7b00326

[19] McGuire, J.A., Sykora, M., Joo, J., Pietryga, J.M. and Klimov, V.I. (2010) Apparent Versus True Carrier Multiplication Yields in Semiconductor Nanocrystals. *Nano Letters*, **10**, 2049-2057. https://doi.org/10.1021/nl100177c

[20] Castañeda, J.A., Nagamine, G., Yassitepe, E., Bonato, L.G., Voznyy, O., Hoogland, S., Nogueira, A.F., Sargent, E.H., Cruz, C.H.B. and Padilha, L.A. (2016) Efficient Biexciton Interaction in Perovskite Quantum Dots Under Weak and Strong Confinement. *ACS Nano*, **10**, 8603-8609. https://doi.org/10.1021/acsnano.6b03908

[21] D'Innocenzo, V., Grancini, G., Alcocer, M.J.P., Kandada, A.R.S., Stranks, S.D., Lee, M.M., Lanzani, G., Snaith, H.J. and Petrozza, A. (2014) Excitons versus Free Charges in Organo-Lead Tri-Halide Perovskites. *Nature Communications*, **5**, Article No. 3586. https://doi.org/10.1038/ncomms4586

[22] Saba, M., Cadelano, M., Marongiu, D., Chen, F., Sarritzu, V., Sestu, N., Figus, C., Aresti, M., Piras, R., Lehmann, A.G., Cannas, C., Musinu, A., Quochi, F., Mura, A. and Bongiovanni, G. (2014) Correlated Electron-Hole Plasma in Organometal Perovskites. *Nature Communications*, **5**, Article No. 5049. https://doi.org/10.1038/ncomms6049

[23] Sestu, N., Cadelano, M., Sarritzu, V., Chen, F., Marongiu, D., Piras, R., Mainas, M., Quochi, F., Saba, M., Mura, A. and Bongiovanni, G. (2015) Absorption F-Sum Rule for the Exciton Binding Energy in Methylammonium Lead Halide Perovskites. *The Journal of Physical Chemistry Letters*, **6**, 4566-4572. https://doi.org/10.1021/acs.jpclett.5b02099

[24] Yang, Y., Yang, M., Li, Z., Crisp, R., Zhu, K. and Beard, M.C. (2015) Comparison of Recombination Dynamics in $CH_3NH_3PbBr_3$ and $CH_3NH_3PbI_3$ Perovskite Films: Influence of Exciton Binding Energy. *The Journal of Physical Chemistry Letters*, **6**, 4688-4692. https://doi.org/10.1021/acs.jpclett.5b02290

[25] Yang, Y., Yan, Y., Yang, M.J., Choi, S., Zhu, K., Luther, J.M. and Beard, M.C. (2015) Low Surface Recombination Velocity in Solution-Grown $CH_3NH_3PbBr_3$ Perovskite Single Crystal. *Nature Communications*, **6**, Article No. 7961. https://doi.org/10.1038/ncomms8961

[26] Yang, Y., Yang, M., Zhu, K., Johnson, J.C., Berry, J.J., van de Lagemaat, J. and Beard, M.C. *et al.* (2016) Large Polarization-Dependent Exciton Optical Stark Effect in Lead Iodide Perovskites. *Nature Communications*, **7**, Article No. 12613. https://doi.org/10.1038/ncomms12613

[27] Manser, J.S. and Kamat, P.V. (2014) Band Filling with Free Charge Carriers in Organometal Halide Perovskites *Nature Photonics*, **8**, 737-743.

[28] Wehrenfennig, C., Eperon, G.E., Johnston, M.B., Snaith, H.J. and Herz, L.M. (2014) High Charge Carrier Mobilities and Lifetimes in Organolead Trihalide Perovskites. *Advanced Materials*, **26**, 1584-1589. https://doi.org/10.1038/nphoton.2014.171

[29] Wehrenfennig, C., Liu, M., Snaith, H.J., Johnston, M.B. and Herz, L.M. (2014) Charge-Carrier Dynamics in Vapour-Deposited Films of the Organolead Halide Perovskite $CH_3NH_3PbI_{3-x}Cl_x$. *Energy & Environmental Science*, **7**, 2269-2275. https://doi.org/10.1039/C4EE01358A

[30] Zhou, H.P., Chen, Q., Li, G., Luo, S., Song, T.B., Duan, H.S., Hong, Z.R., You, J.B., Liu, Y.S. and Yang, Y. (2014) Interface Engineering of Highly Efficient Perovskite Solar Cells. *Science*, **345**, 542-546. https://doi.org/10.1126/science.1254050

[31] de Quilettes, D.W., Vorpahl, S.M., Stranks, S.D., Nagaoka, H., Eperon, G.E., Ziffer, M.E., Snaith, H.J. and Ginger, D.S. (2015) Impact of Microstructure on Local Carrier Lifetime in Perovskite Solar Cells. *Science*, **348**, 683-686. https://doi.org/10.1126/science.aaa5333

[32] Price, M.B., Butkus, J., Jellicoe, T.C., Sadhanala, A., Briane, A., Halpert, J.E., Broch, K., Hodgkiss, J.M., Friend, R.H. and Deschler, F. (2015) Hot-Carrier Cooling and Photoinduced Refractive Index Changes in Organic-Inorganic Lead Halide Perovskites. *Nature Communications*, **6**, Article No. 8420. https://doi.org/10.1038/ncomms9420

[33] Liu, J., Leng, J., Wang, S., Zhang, J. and Jin, S. (2019) Artifacts in Transient Absorption Measurements of Perovskite Films Induced by Transient Reflection from Morphological Microstructures. *The Journal of Physical Chemistry Letters*, **10**, 97-101. https://doi.org/10.1021/acs.jpclett.8b03704

[34] Tian, Y. and Scheblykin, I.G. (2015) Artifacts in Absorption Measurements of Organometal Halide Perovskite Materials: What Are the Real Spectra? *The Journal of Physical Chemistry Letters*, **6**, 3466-3470. https://doi.org/10.1021/acs.jpclett.5b01406

[35] Cong, L., Srivastava, Y.K., Solanki, A., Sum, T.C. and Singh, R. (2017) Perovskite as a Platform for Active Flexible Metaphotonic Devices. *ACS Photonics*, **4**, 1595-1601. https://doi.org/10.1021/acsphotonics.7b00191

[36] Ishioka, K., Barker, B.G., Yanagida, M., Shirai, Y. and Miyano, K. (2017) Direct Observation of Ultrafast Hole Injection from Lead Halide Perovskite by Differential Transient Transmission Spectroscopy. *The Journal of Physical Chemistry Letters*, **8**, 3902-3907. https://doi.org/10.1021/acs.jpclett.7b01663

[37] Makarov, N.S., Guo, S., Isaienko, O., Liu, W., Robel, I. and Klimov, V.I. (2016) Spectral and Dynamical Properties of Single Excitons, Biexcitons, and Trions in Cesium-Lead-Halide Perovskite Quantum Dots. *Nano Letters*, **16**, 2349-2362. https://doi.org/10.1021/acs.nanolett.5b05077